Probing interfacial interactions and dynamics of polymers enclosed in boron nitride nanotubes

*Jukka Niskanen, Yanming Xue, Dmitri Golberg, Françoise M. Winnik, Christian Pellerin, and Jaana Vapaavuori**

Dr. Jukka Niskanen
Université de Montréal, Département de Chimie, C.P. 6128, Succursale Centre-Ville, Montréal, QC, H3C 3J7, Canada

jukka.niskanen@icloud.com

Prof. Yanming Xue
International Center for Materials Nanoarchitectonics (MANA), National Institute for Materials Science (NIMS), 1-1 Namiki, Tsukuba, Ibaraki 305-0044, Japan

School of Materials Science and Engineering, Hebei University of Technology, Tianjin 300130, P.R. China

ym.xue@hebut.edu.cn

Prof. Dmitri Golberg
International Center for Materials Nanoarchitectonics (MANA), National Institute for Materials Science (NIMS), 1-1 Namiki, Tsukuba, Ibaraki 305-0044, Japan

Centre for Materials Science and School of Chemistry and Physics, Queensland University of Technology (QUT), 2 George Street, Brisbane, QLD 4000, Australia

dmitry.golberg@qut.edu.au

Prof. Françoise M. Winnik
International Center for Materials Nanoarchitectonics (MANA), National Institute for Materials Science (NIMS), 1-1 Namiki, Tsukuba, Ibaraki 305-0044, Japan

Laboratory of Polymer Chemistry, Department of Chemistry, University of Helsinki, P.O. Box 55, 00014 Helsinki, Finland

francoise.winnik@helsinki.fi

Prof. Christian Pellerin
Université de Montréal, Département de Chimie, C.P. 6128, Succursale Centre-Ville, Montréal, QC, H3C 3J7, Canada

c.pellerin@umontreal.ca

Prof. Jaana Vapaavuori
Université de Montréal, Département de Chimie, C.P. 6128, Succursale Centre-Ville, Montréal, QC, H3C 3J7, Canada

Department of Chemistry and Materials Science, Aalto University, P.O. Box 16100, FI-00076 AALTO, Finland

jaana.vapaavuori@aalto.fi

Present Addresses

Dr. Jukka Niskanen
VTT Technical Research Centre of Finland Ltd
P.O. Box 1000, FI-02044 VTT, Finland

Prof. Yanming Xue
[a]School of Materials Science and Engineering, Hebei University of Technology, Tianjin 300130, P.R. China. [b]Hebei Key Laboratory of Boron Nitride and Nano Materials, Hebei University of Technology, Tianjin 300130, P.R. China.

Keywords: Glass Transition Temperatures, Photoactive Polymers, Loading Nanotubes, Infrared Spectroscopy

Abstract

Understanding interfacial interactions in polymer systems is crucial for their applicability for instance in adhesives and coatings. Enclosing polymers in a cylindrical volume provides a system for studying interactions dictated by a continuous interfacial layer and a bulk-like volume in the middle of the cylinders. Here, we describe a simple method for enclosing polymers into boron nitride nanotubes (BNNTs) and establishing the effect of the interfacial interactions on the glass transition temperature (T_g) of the polymers by infrared spectroscopy. The volume of the inner channel is large in comparison to the volume of the loaded polymer coils, allowing the polymer to expand along the inner channel, resulting in the effect of interfacial interactions on polymer dynamics dominating over confinement effects. As examples, we loaded poly(4-vinyl pyridine), poly(methyl methacrylate), poly(vinyl pyrrolidone), and poly(disperse red 1 acrylate) in BNNTs. The strongest interaction between the studied polymer and BNNTs was observed for poly(4-vinyl pyridine), which also caused a

significant increase of T_g. In addition to characterizing the effect of interfacial interactions on the thermal transitions of the polymers, this method, which is generalizable to most soluble polymer materials, can be used for studying photoinduced transitions in photoactive polymers thanks to the transparency of the BNNTs at visible wavelengths.

1. Introduction

Polymers in enclosed spaces are common in our everyday lives, from adhesives, lubrication systems, and coatings to biological microstructures.[1,2] In these cases, the importance of interfacial interactions between the confining surface and the polymer becomes more and more dominant with decreasing volume of the cavity. Thin films (15-300 nm) of polymers (poly(isobutyl methacrylate) and polystyrene) on a flat silicon surface have been modelled as consisting of three regions with different viscosities: an interfacial layer adjacent to the substrate, a bulk-like intermediate layer, and a top mobile layer (second interfacial layer), as determined from polymer diffusivity data obtained from fluorescence recovery after patterned photobleaching.[3] Furthermore, localized T_g measurements have shown that there is a gradient of T_g ranging from the free surface to tens of nm deep in the interior of a thin film.[4,5] To complicate things further, the diverse ways in which different measurement techniques average this phenomenon into one single T_g makes it difficult to directly compare results for thin nanoconfined films. In addition, trapping polymers in spaces comparable to their molecular dimensions (< 100 nm) can alter their physical properties as compared to those in the bulk.[3,6–10] Computational modeling has shown that the radius of gyration of linear or star polymers decreases upon squeezing them between two walls, as the polymer conformation changes from three-dimensional to virtually two-dimensional.[2]

Even when taking into account the above-mentioned experimental challenges, a majority of the work dedicated to the impact of interfacial interactions and spatial confinement on glass

transition, diffusivity, effective viscosity, and related mechanical properties of polymer films, has been done in planar geometries in which films are either free-standing, supported by a solid substrate from one side, or squeezed in between the surfaces of two similar or dissimilar planar substrates. Even though seemingly contradictory results have been obtained, potentially partially related to the difficulty in comparing the results coming from different indirect measurement methodologies,[11] there is ample evidence that surfaces and interfaces modify the polymer dynamics relevant to glass transition in the intermediate regions of polymers.[12] The method we introduce here, the confinement of polymers in a cylindrical volume, eliminates the problems of having two interfacial layers with differing interfacial interactions and thus allows us to examine the impact of a single defined interface on polymer dynamics.

Attenuated total reflection infrared (ATR-IR) spectroscopy is a simple and broadly available sampling method that provides chemical selectivity for probing supramolecular interactions in structured materials. It readily allows temperature-controlled measurements to determine spectroscopic T_g values, due to the discontinuity in the coefficient of the thermal expansion coefficient at T_g that often leads to band shifts with a second order-like temperature dependence, including when the polymer is spatially confined.[13–21] Moreover, this data can be directly correlated by the temperature behavior of the supramolecular interactions at the interface between the amorphous polymer and confining material surface. ATR-IR can also be combined with in situ irradiation or other types of sample perturbations to probe their impact on polymer interactions or dynamics. Herein, we chose to load polymers in boron nitride nanotubes (BNNT), with a diameter of 44 nm, to study the thermal behavior of several polymers and their interfacial supramolecular interactions.[22] BNNTs are structural analogues of carbon nanotubes (CNT), with excellent mechanical and chemical stability, high thermal conductivity, and low thermal expansion coefficient (3.5×10^{-5} K^{-1}).[23–27] In addition,

BNNTs have only a few IR absorption bands that leave open large spectral windows to study the characteristic polymer absorption bands.[28]

Due to the delocalization of electrons over the boron-nitrogen bonds, BNNTs interact strongly with nitrogen-containing compounds.[29–33] Amines are bound from their electron-rich nitrogen to the electron deficient boron atoms of the BNNTs by coordination bonds (E_{ads} = -32.8 to -92.6 kJ/mol).[34–37] Hence, proteins and polymers containing amines have a high affinity towards BNNTs.[7,10] For comparison, proteins and amino acids bind to CNT by far weaker hydrophobic and van der Waals interactions.[38] Glycine and ethanolamine has been used as non-destructive aids to disperse the hydrophobic BNNTs in various media.[29,39–41] Stable dispersion of the BNNTs also provided an opportunity to cut and load them with compounds.[29,39,40,42] Other dispersion methods are less favorable since they use harsh oxidative conditions that damage the BNNTs.[42–51] Thus, for our study, BNNTs form an enclosing surface capable of accepting coordination bonds, and thus immobilizing electron donating chemical groups.

To demonstrate the generalizability of our method and to investigate the effect of interfacial interactions on the T_g, we measured the spectroscopic T_g of several polymers: poly(4-vinyl pyridine) (P4VP), poly(methyl methacrylate) (PMMA), poly(vinyl pyrrolidone) (PVP), and poly(disperse red 1 acrylate) (PDR1A) loaded in BNNTs. P4VP, PDR1A, and PVP all have nitrogen atoms, which can strongly interact with the BNNTs, whereas PMMA contains no groups (aromatic or amino) expected to form specific chemical interactions with the BNNTs. Our results show that for P4VP, which interacts strongly with the surface of the BNNTs, the T_g was initially higher in the BNNTs than what was observed for free polymer. Our method provides a possibility to simultaneously follow the nature and the strength of supramolecular

interactions to T_g, has a comparative advantage to state-of-the art measurements of T_g by differential scanning calorimetry.

2. Results and discussion

2.1 BNNTs loaded with polymers

Liquids with a low surface tension can readily enter cut BNNTs. The loading, illustrated in **Figure 1**A, is governed by capillary forces, which are affected by the surface tension of the liquid and the wetting of the BNNT inner walls. Evidently, the chosen solvent should be a good solvent for the loaded substance and additionally, the solvent should also solubilize atmospheric gases trapped inside the BNNTs. Therefore, reducing the pressure eases the filling of halloysite, CNTs, and BNNTs with liquids.[40,52–56] Chloroform (for P4VP), methanol (for PVP), or tetrahydrofuran (for PMMA and PDR1A) were used for solubilizing and loading the polymers in BNNTs. All these solvents have low surface tensions (27.5, 22.7, and 26.4 mN/m, respectively). The concentration of the polymer solution should be as high as possible to increase polymer loading in the BNNTs, yet low enough so that viscosity does not preclude penetration of the solution within the tubes. As a compromise, we kept the polymer concentrations at 200 mg/mL.

The loading of the polymers in ethanolamine-functionalized Cut-BNNTs was confirmed by TEM (Supporting Information, Figure S1). The ethanolamine functionalization is a simple method to increase the dispersibility of BNNTs in various solvents, a vital step to cut and load the BNNTs.[41] We chose to use ethanolamine over glycine so that the BNNTs would not become negatively charged by the glycine,[29] to avoid ionic interactions between the nitrogen containing polymers and the BNNTs. FT-IR of the samples show no characteristic absorbance bands for ethanolamine (N-H bending at 1665 cm^{-1} and C-N stretching at 1065 cm^{-1}) after the loading process with excessive washing and sonication (Supporting Information, Figure S2).

Hence, the interactions between the boron atoms in the BNNTs and the polymers will be dominant over possible hydrogen bonding between remaining ethanolamine and the polymers. The absence of interactions between PMMA and the BNNTs, discussed later in this paper, confirms that interactions originating from ethanolamine are negligible. However, the FT-IR absorbance bands will include both the thin layer of polymer outside the BNNTs, as well as the polymer inside the BNNTs. Dark sections, separated by lighter sections, can be observed in the TEM micrograph of Figure 1C for BNNTs loaded with PMMA and Supporting Information Figure S1 for BNNTs loaded with the four polymers. The dark sections represent the dry polymer separated by air. It should be noted that the menisci of the polymers are concave, indicating that the solvents were able to wet the surface, analogously to when BNNTs are loaded with small molecular compounds.[40–42]

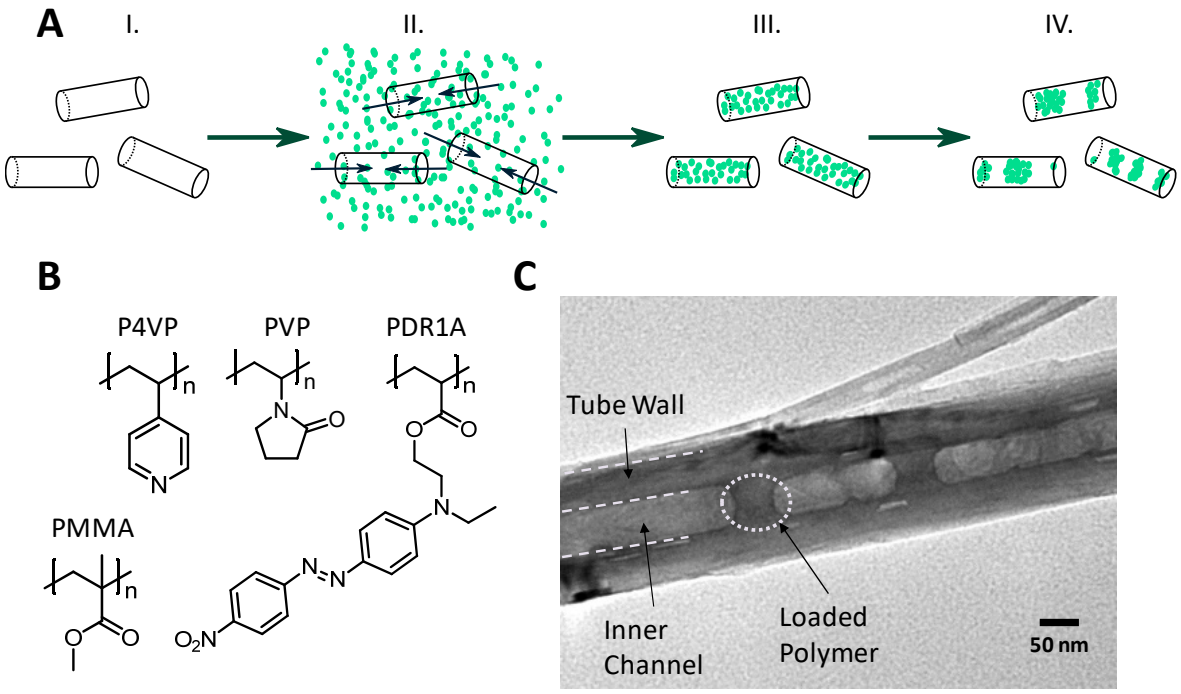

Figure 1. A. Scheme of the loading process under reduced pressure: (I) Cut BNNTs, (II) BNNTs dispersed in a polymer solution under reduced pressure, (III) loaded BNNTs after washing, and (IV) loaded BNNTs after drying *in vacuo*. **B.** Chemical structures of the

polymers loaded in BNNTs. **C.** TEM micrograph visualizing polymer (PMMA) loaded inside a BNNT.

2.2 IR investigations of polymers loaded in BNNTs

The presence of the polymers can be observed in the IR spectra of the loaded BNNTs. In contrast, bands characteristic of the solvents used in the loading process were not observed (**Figure 2**). The formation of interactions between P4VP and the BNNTs at low temperature (40 °C) is revealed by the presence of a shoulder at 1008 cm^{-1} on the 993 cm^{-1} band (Figure 2B). For comparison, in the spectra of pure P4VP, no shoulder can be observed on the 993 cm^{-1} band (Figure 2C). Other views are provided in Figure S3 of the Supporting Information.

The 993 cm^{-1} pyridine band is known to shift to higher position upon hydrogen bonding, halogen bonding with a donating group, protonation, or participation in a charge-transfer complex, with the magnitude of the shift depending on the strength of the interaction.[57,58] Wang et al. used the intensities of the 993 and 1008 cm^{-1} bands to calculate the fraction P4VP hydrogen bonded to 4,4'-biphenol.[59] The shoulder observed at 1008 cm^{-1} thus indicates a partial supramolecular binding of the polymer from the nitrogen in P4VP to a boron atom in the BNNTs. Increasing the temperature to 160 °C provokes a strong decrease of this shoulder so that it can be concluded that these supramolecular interactions can be mostly broken by heating the sample.

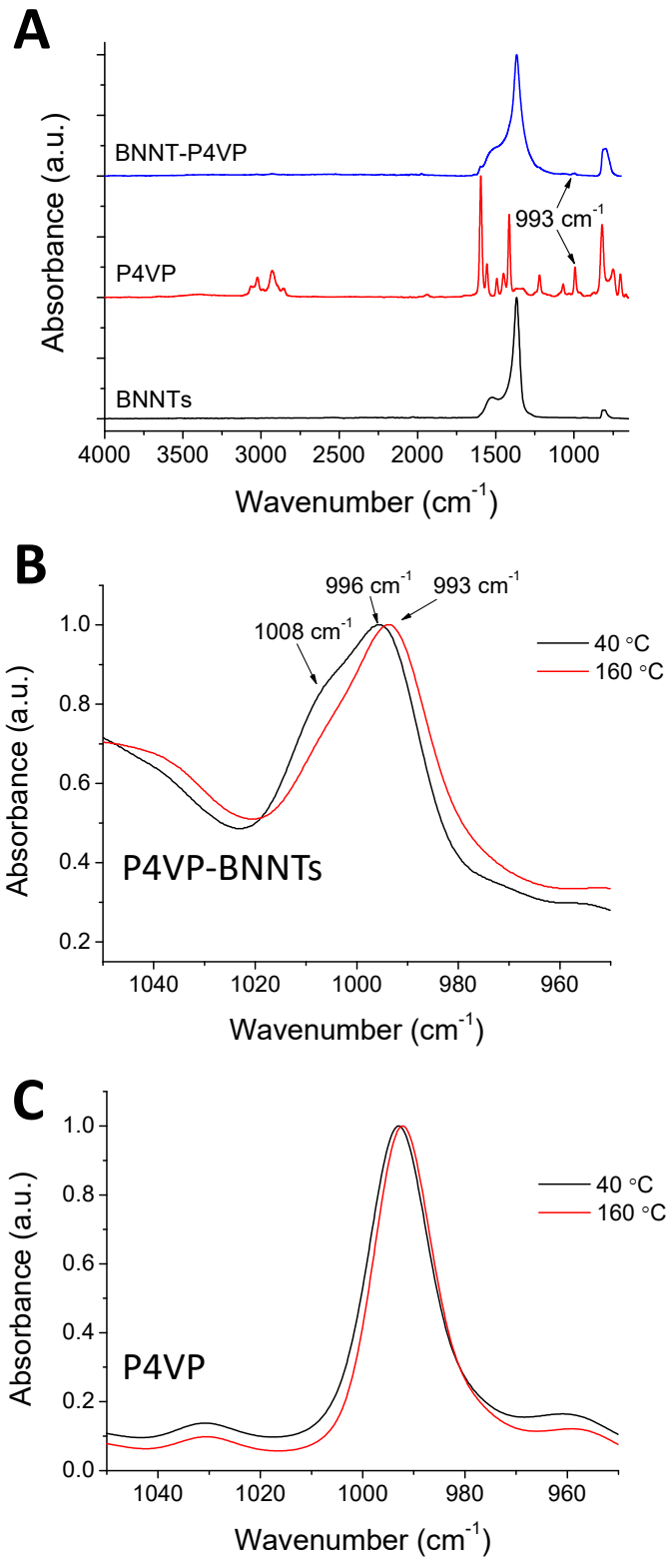
A
Absorbance (a.u.)
BNNT-P4VP
P4VP
BNNTs
993 cm-1
4000 3500 3000 2500 2000 1500 1000
Wavenumber (cm-1)
B
996 cm-1
993 cm-1
1008 cm-1
40 °C
160 °C
Absorbance (a.u.)
P4VP-BNNTs
1.0 0.8 0.6 0.4 0.2
1040 1020 1000 980 960
Wavenumber (cm-1)
C
40 °C
160 °C
Absorbance (a.u.)
P4VP
1.0 0.8 0.6 0.4 0.2 0.0
1040 1020 1000 980 960
Wavenumber (cm-1)

Figure 2. IR spectra of BNNTs, P4VP, and BNNT-P4VP (A), P4VP-loaded BNNTs showing evidence of temperature-dependant intermolecular interactions (1008-cm^{-1} shoulder, B). Only minute changes are observed for pure P4VP (C).

Considering the weakness of the polymer bands in the IR spectra (Figure 2A), it is essential to optimize the sampling volume to obtain reliable measurements. Considering that the radius of the tubes is 22 nm, the loaded polymer can be thought of as the equivalent of a 22 nm thin film on a boron nitride surface, but rolled up inside a cylindrical geometry. This leads to a clear sampling advantage compared to a thin film geometry because several layers of BNNT can be piled up in the sampling volume, instead of a single one, while preserving the ultrathin film conditions. If we assume that a thickness of 1.9 μm is probed (considering the penetration depth of the ATR under the conditions used), that the dried BNNT dispersion occupies only 50 % of the sampled volume, and that the polymer chains only fill 25 % of the BNNT, the polymer content in the sampled volume is approximately 10 times in BNNTs compared to a planar thin film.

BNNTs have three strong absorption bands at 807, 1367, and 1522 cm^{-1} (Figure 2A). The band at 807 cm^{-1} can be attributed to B-N vibration perpendicular to the BNNT axis and the bands at 1367 and 1522 cm^{-1} to longitudinal and transverse in-plane stretching modes, respectively.[60–62] The 1367 and 1522 cm^{-1} bands overlap with several of the bands originating from P4VP. However, the pyridine ring deformation at 993 cm^{-1} is visible and does not overlap with BNNT bands (Figure 2).

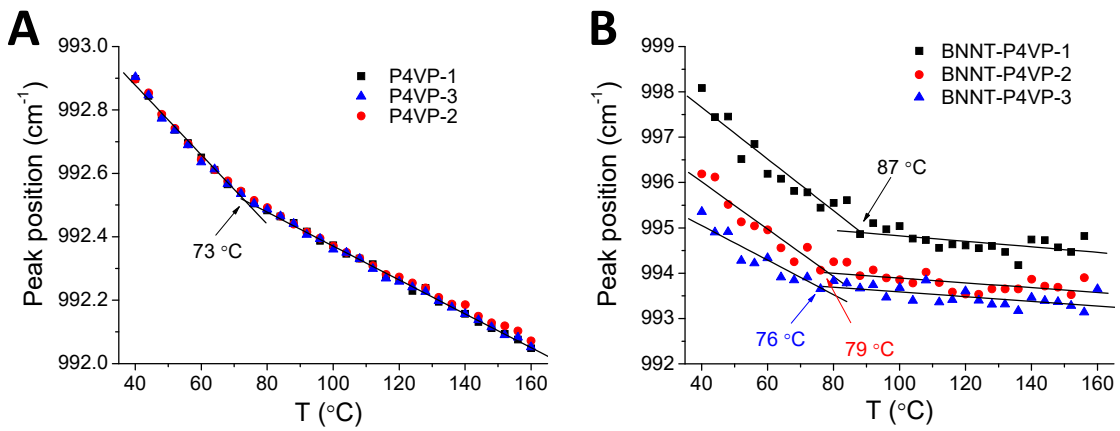

Figure 3. The position of the pyridine deformation band at 993 cm^{-1} for P4VP (A) and BNNT-P4VP (B) as a function of temperature for three temperature ramps of a sample, with the T_g indicated for each ramp. The change in the slope of the peak position indicates the glass transition temperature for the polymer.

The 993 cm^{-1} band was used to determine the T_g of pure P4VP and BNNT-P4VP, from three temperature ramps of the same sample. In both cases, the band shifts almost linearly to lower wavenumbers with increasing temperature until there is a change of the slope in the linear decrease at the glass transition temperature, which can be determined from the intersection of two lines fitted to the data points (**Figure 3**). The spectroscopic T_g of P4VP was determined as 73 °C (Figure 3A and **Table 1**) while the T_g of BNNT-P4VP was observed to be significantly higher at 87 °C (Figure 3B), but to gradually decrease from 87 to 76 °C from the first to the third heating cycle. In contrast, no change in the T_g was observed for the pure polymer between three consecutive ramps (Figure 3A). The average band position was shifted from 993 (P4VP) to 998 cm^{-1} (BNNT-P4VP) at 40 °C due to the presence of the high-wavenumber shoulder due to pyridine interactions with the BNNT surface. The 993 cm^{-1} pyridine band is known to shift to higher wavenumbers upon interactions of the pyridine ring with electron acceptors.[57,63,64] Interestingly, the position of this band shifts to lower wavenumbers with

each consecutive run, indicating that the polymer is in a metastable state after the loading procedure, and that the fraction of pyridine rings interacting with the BNNT surface decreases when the polymer rearranges in the BNNTs (Supporting Information, Figure S3).

Polymers containing amines are bound to BNNTs from the electron-rich nitrogen to the electron deficient boron atoms of the BNNTs.[30,33–37] The high adsorption energies (E_{ads} = -32.8 to -92.6 kJ/mol) indicate that the formed coordination bonds are of chemical nature and the binding energy increases with the number of amino groups.[34] Conjugated polymers and compounds are also bound to BNNTs via π–π interactions, which can facilitate charge transfer between the BNNTs and the polymers.[65–69] In the case of BNNT-P4VP, both coordination bonding and π–π interactions are present. Upon heating BNNT-P4VP above its T_g the polymer rearranges itself. The interactions between the pyridine ring and boron nitride are broken by the thermal motion and replaced by intra and intermolecular interactions with neighboring polymers. This rearrangement is seen as a decrease in the T_g of the material, a shift in the position of the band at 993 cm^{-1}, and the strong attenuation of the shoulder at 1008 cm^{-1}. Upon cooling the mobility of the polymers is reduced and the reformation of BNNT-P4VP bonding is less likely to occur. It should also be noted that the polymers were introduced into the BNNTs as a solution, and during the evaporation of the solvent polymer chains were spread along the BNNT surface leaving the polymer in a metastable state.

Jiang et al. showed recently how the T_g of polymers is increased by polymer-solid interactions, due to the interactions slowing down molecular movement of the adsorbed polymers.[70] They observed that the T_g of poly(2-vinyl pyridine) (P2VP) in a thin film on SiO_2 is radically higher for the polymers that interact with the SiO_2 surface compared to the other parts of the film. The T_g of the P2VP adhered to the SiO_2 was 203 °C, whereas the T_g for the bulk-like layer in the P2VP film was 98 °C.[70] A similar change in T_g was also observed

for polystyrene. These observations loosely resemble what we found for P4VP in BNNTs. Jiang et al. have also shown that the annealing of flattened and adhered polymers on a surface, above the T_g of the bulk polymer, causes the interaction between the polymers and the surface to change and to provoke the formation droplet-like structures. They also concluded that the droplet-forming process is affected by the interfacial interactions.[70,71] In our case, the change in the interactions between P4VP and the BNNT surface due to annealing can be seen as a decrease in the T_g from 87 to 76 °C for BNNT-P4VP between consecutive heating cycles.

Polymers can also be trapped in metastable states on a surface after annealing the polymer. Polystyrene has been shown to spread along an aluminum surface during long annealing (50 min).[72] P4VP interacts strongly with the tube surface, hence we can expect the polymer to be kinetically trapped in a metastable state before the first heating. On heating the polymer above its T_g, the coils gradually tend toward their equilibrium state. However, this relaxation process is slow and the T_g approaches the value of bulk P4VP only after three heating cycles. Hence, the spreading of polymers along the tube surface during the anneal is expected to be negligible.

We also note that although we observe a slight increase in the T_g of BNNT-P4VP compared with bulk P4VP, an increase in T_g is not granted for thin films along solid interfaces. For instance, Chen et al. reported an 8-10 °C (2%) lower T_g for a 15 nm thick polystyrene film compared to the T_g of bulk, due to entropy of the film body. [73]

Material	T_g (°C)	
	DSC	IR
P4VP	89 (±1)	73 (±1)
BNNT-P4VP	-	81 (±6)
PMMA	114 (±1)	108 (±3)
BNNT-PMMA	-	111 (±1)
PVP	116 (±1)	67 (±2)
BNNT-PVP	-	63 (±2)
PDR1A	85*	83 (±1)

Table 1. Comparison of the glass transition temperatures (T_g) of P4VP, BNNT-P4VP, PMMA, BNNT-PMMA, PVP, BNNT-PVP, and PDR1A determined by DSC or IR spectroscopy. *The T_g of PDR1A measured by DSC was reported previously by Vapaavuori et al.[21]

The T_g of PMMA was determined to be 108 °C from the IR spectra for three different samples of the polymer (**Figure 4**), close to what was measured by DSC (114 °C). The T_g of PMMA loaded in the BNNTs was determined to be 111 °C for two samples (Supporting Information, Figure S4). As discussed in Supporting Information, similar results were obtained for pure PMMA using shifts in band position and changes in band intensity, but the former provided more easily quantifiable results for BNNT-PMMA.

A slight shift to lower wavenumbers (0.4 cm^{-1}) of the carbonyl band is observed for BNNT-PMMA, in comparison to PMMA. The position of the carbonyl stretching band is sensitive to interactions and is observed to shift by several wavenumbers to lower values in the presence of electron deficient compounds.[74,75] In addition, both measured T_g values for PMMA (108 °C) and BNNT-PMMA (111 °C) are within the error margins (±3 °C) of the method. This small shift of the band indicates that there are no strong interactions between PMMA and the

BNNTs nor between PMMA and any remaining ethanolamine on the surface of the BNNTs. Since this observation correlates well with the polymers T_g being independent of whether in bulk or enclosed in a nanotube (as well as the T_g in the nanotube not changing between the number of heating cycles), we have further evidence for that the observed effect on the T_g for P4VP is due to the stronger supramolecular interaction hindering the polymer dynamics, not due to nanoconfinement effect.

The PMMA was synthesized via ATRP, for controlled synthesis with regards to molecular weight distribution, but also of the end groups. The initiating species in the synthesis leaves the PMMA with an ethyl ester at one end of the polymer and a tertiary haloalkane (bromine) at the other end. Neither of them is expected to have strong interactions with the nanotubes, hence the PMMA will not be tethered from the end groups to the nanotubes. Similarly, a tethering effect by the end groups (alkane and phenyl groups) is not expected to occur for the above-described BNNT-P4VP system, based on the information provided by the P4VP supplier.

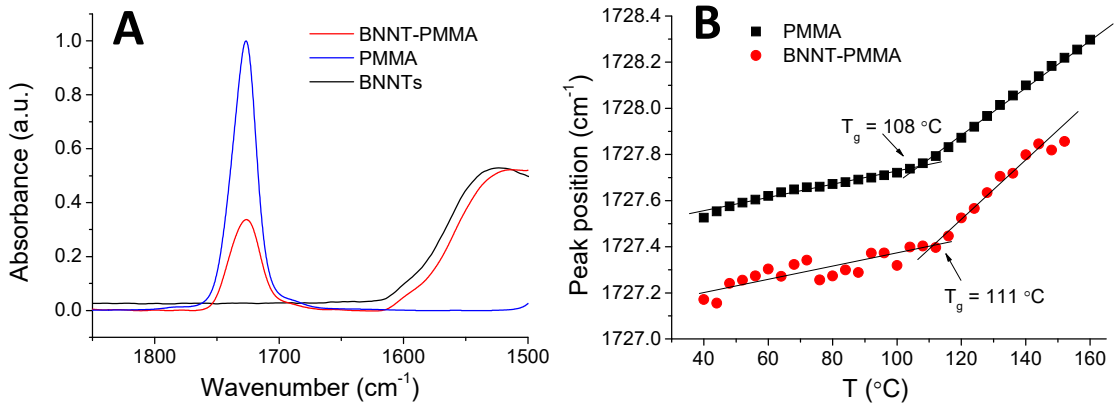

Figure 4. Carbonyl stretching region of the IR spectra of BNNTs, PMMA, and BNNT-PMMA (A), and the position of the carbonyl stretching band of PMMA as a function of temperature (B), with the T_g indicated for the pure PMMA and BNNT-PMMA samples.

Heating a sample in a condensed phase usually leads to a reduction in its intermolecular interactions because of increases in specific volume and random molecular motions. An exception to this is when cold crystallization occurs on heating above T_g, which is not the case for atactic PMMA. In the case of carbonyl groups, dipole-dipole interactions tend to decrease the force constant of the C=O bond, which in turn tends to decrease the frequency of the carbonyl stretching band. Conversely, reducing these interactions by heating the sample tends to increase the force constant and thus the wavenumber at which the band appears (Figure 4B). The effect observed is small because the dipole-dipole interactions are weak compared to stronger intermolecular interactions such as hydrogen bonds. For example, the carbonyl stretching band of PMMA was found to shift by 26 cm^{-1} toward lower wavenumbers upon forming H-bonds with poly(vinylphenol).[76]

The T_g of PVP and BNNT-PVP were determined as 67 and 63 °C, respectively, from the IR spectra (**Figure 5**). These values are significantly lower than the T_g of 116 °C determined by DSC. PVP is a very hygroscopic polymer and the absorption of water into the polymer is known to significantly decrease its T_g.[77] The samples were drop-casted on the ATR-crystal from a solution in methanol and the water absorbed, from air and methanol, into the polymer during the evaporation of the solvent could not be removed by heating the sample to 160 °C. Characteristic bands for water are observed at 3400 cm^{-1} (Supporting Information, Figure S5).

The Amide I band of PVP, observed at 1679 cm^{-1} in PVP-BNNT (Supporting Information, Figure S6), is a combined mode of C=O and C-N stretching, and dipole-dipole interactions or

hydrogen bonding are both known to shift this band.[78] In our case, hydrogen bonds between residual water and PVP dominate over interactions between PVP and the BNNTs.

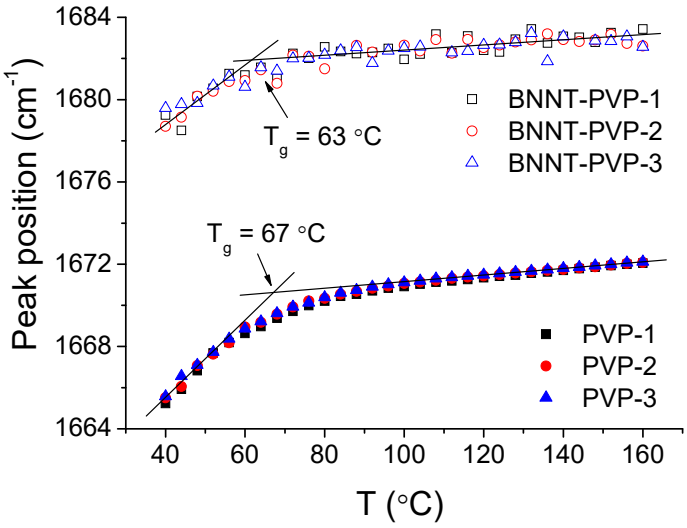

Figure 5. The Amide I band position of BNNT-PVP and PVP as a function of temperature for three temperature ramps of a sample, with the T_g indicated.

The C-H in-plane bending and ring deformation combined with C-N stretching absorbance bands of photoresponsive azobenzene containing PDR1A, observed at 1102 and 1128 cm^{-1}, shift to 1106 and 1135 cm^{-1} when the polymer is loaded inside the BNNTs (**Figure 6**A), which is an indication of the polymer interacting with the BNNTs. Both bands are known to be affected by photoisomerization but also from the azobenzene group interacting with its environment. In the case of BNNT-PDR1A, the absorption band at 1106 cm^{-1} is slightly more prominent at 40 °C, compared to the sample being heated to 160° (Figure 6B). Indicating the polymer interactions between PDR1A and the BNNTS are weaker at 160 °C than at 40 °C. The T_g of BNNT-PDR1A could not be determined from the IR spectra due to overlapping of the absorbance bands resulting in scattering of the data points (Supporting Information, Figure S7 and S8). However, the T_g of the PDR1A polymer was measured by IR as 83 °C and recently by DSC as 85 °C.[21]

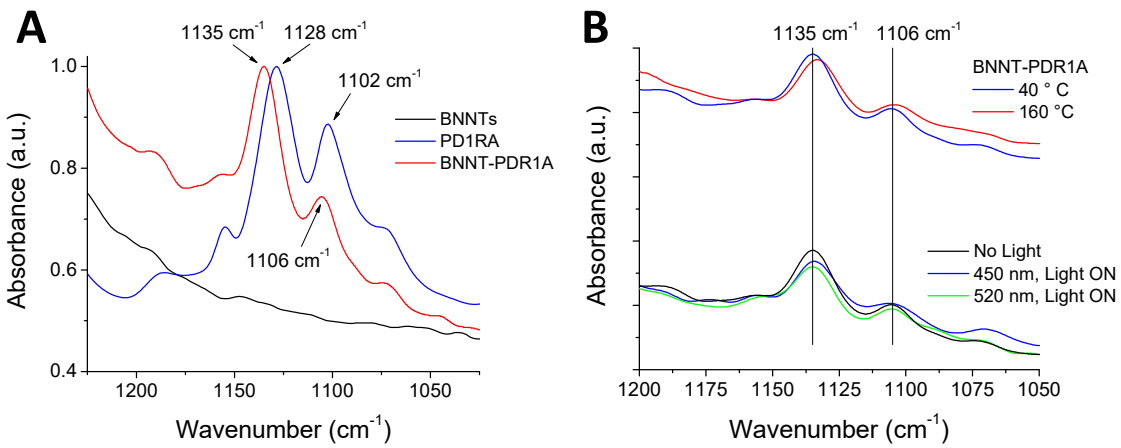

Figure 6. Close up of the C-H in-plane bending and ring deformation absorbance band position of PDR1A (A), the same absorbance bands at 40 and 160 °C (top, B), and upon illumination with 520 and 450 nm light at 40 °C (bottom, B).

Photoisomerization of the azobenzene in PDR1A can be induced illuminating by both 450 nm and 520 nm light. Due to the transparency of the BNNTs at these wavelengths, we were able to observe photoisomerization in-situ by following the 1135 cm^{-1} absorption band, which is slightly diminished and broadened upon illumination, as indicated by Figure 6B. The absorption intensity of the 1106 and 1135 cm^{-1} bands have been shown to decrease upon light induced photoisomerization of the azobenzene to *cis*-configuration.[79,80] The broadening of the 1106 cm^{-1} band caused by 450 nm light is similar to what could be observed by heating the sample. This broadening of the 1106 cm^{-1} band could be reversed by 520 nm light (or by cooling). Hence, either heat or light could be used to change the interactions or conformation of the azobenzene groups loaded in BNNTs. This implies that the BNNTs can also be used as model systems for studying the effect of interfacial interactions on the photoresponse of the polymer, since the BNNTs are transparent cages at 450 and 520 nm.[81]

As demonstrated by this paper, four different polymer materials were successfully enclosed in BNNTs, and we expect this strategy to be generalizable to all soluble polymer materials. The

major advantage is that the presented method takes advantage of the vibrational modes, while carrying information about the physical molecular environment, directly linked to the glass transition temperature of the material, and the chemical interactions of that specific group. Hence, the interfacial interactions and the polymer dynamics can be simultaneously measured with one simple and accessible method, thus contributing directly to the debate of establishing the relationship between these two important phenomena.

The curvature of a surface has been reported to increase the observed T_g of polystyrene. As the curvature of the surface is increased for thin films of PS (11-23 nm), the T_g increased from 88 °C (bulk) to 106 °C (thin film on a 55 nm diameter cavity).[82] We do observe a small increase in the T_g of P4VP and PMMA inside the BNNTs compared to the bulk. However, the polymer in the BNNTs is present as filled sections with cylinder-like dimensions, compared to thin films along the walls of a cylinder. We cannot exclude the effect of the curvature of the surface on the T_g, as this study is limited to one sized BNNTs. Due to the small changes in T_g, it is likely that other phenomena than the curvature of the BNNTs dominate. If the effect of curvature inside the BNNTs is negligible, then the lower curvature of the outside surface of the BNNTs should have an even smaller effect.

3. Conclusions

In this article, we demonstrate how temperature-controlled vibrational spectroscopy can be employed on polymers enclosed in boron nitride nanotubes (BNNTs) to simultaneously study their supramolecular interfacial interactions and thermal transitions. Only one material-material interface present in the nanotube, which simplifies resolving the contribution of the interfacial interaction from the polymer dynamics as compared with the case of conventional nanoconfined (ultra)thin films where two dissimilar interfaces must be taken into consideration. Two different scenarios are showcased to demonstrate this methodology. On

one hand, polymers making significant supramolecular interactions to BNNT surface present different dynamics, as directly observed by an increase in T_g. On the other hand, a model polymer for which supramolecular interactions to BNNT are not observed via infrared spectroscopy maintains an unchanged T_g upon enclosure into BNNTs. This simple method should be generalizable to any soluble polymer material and, thanks to the transparency of the BNNTs at visible wavelengths, it can also be used to probe photoinduced transitions in enclosed photoactive polymers. A key advantage of the method is that it can simultaneously probe the chemical and physical environment of a specific molecular group, thus giving a direct handle for establishing the effect of the interfacial interaction on the thermal transitions in soft materials.

4. Experimental

4.1 Materials

Methyl methacrylate (98%) was distilled under reduced pressure. Acetone, chloroform (HPLC) copper(I) bromide (99.998%), cyclohexanone, ethanolamine (98%), ethyl-2-bromoisobutyrate (98%), 1,1,4,7,10,10-hexamethyltriethylenetetramine (HMTETA, 97%), isopropanol, methanol, poly(vinyl pyrrolidone) (PVP, 10 000 g/mol), tetrahydrofuran (THF, 99.9%), and poly(disperse red 1 acrylate) (PDR1A, 5000 g/mol) were obtained from Sigma-Aldrich and used as received. Poly(4-vinyl pyridine) (P4VP, 3200 g/mol, PDI 1.2) was obtained from Polymer Source and used as received. High-purity multiwalled BNNTs were synthesized by boron oxide-assisted chemical vapor deposition (BOCVD) as reported previously.[23]

4.2 Cut BNNTs

BNNTs were cut by sonication in a Qsonica Q700 sonicator as follows.[41] The BNNTs (74 mg) were dispersed in isopropanol (100 mL) by sonication (90% amplitude) pulsing the

sample with 15-second bursts of sonication and with 15-second intervals for a total of 1 min sonication time. Ethanolamine (22 mL) was added to the dispersion and the same procedure was repeated. The excess of ethanolamine was removed by separating the BNNTs from the dispersion by centrifugation (14 000 rpm, 1 min). The BNNTs were dispersed in isopropanol (40 mL) and the flask was placed in a bath of dry ice/isopropanol to prevent the solvent from evaporating during the sonication. The BNNTs were sonicated using 75% amplitude, cycling 15 seconds on and off, for a total sonication time of 2 hours. The average length and diameter of the BNNTs was determined from TEM micrographs (Supporting Information, Figure S2 and S9) as 2.3 (± 0.8) μm and 44 (± 3) nm.

4.3 Poly(methyl methacrylate)

The polymerization of methyl methacrylate was conducted as follows by adjusting previously described ATRP (atom transfer radical polymerization).[83,84] CuBr (72.4 mg, 0.50 mmol) was placed in a vial. In another vial, cyclohexanone (1.0 mL) and 1,1,4,7,10,10-hexamethyltriethylenetetramine (132 μL, 0.49 mmol) were placed. Both vials were sealed, and the vials were flushed with nitrogen gas. After 20 min, contents of the two vials were combined under nitrogen atmosphere. In a separate flask, ethyl-2-bromoisobutyrate (132.9 mg, 0.68 mmol) and methyl methacrylate (3.74 g, 37.4 mmol) were dissolved in cyclohexanone (2 mL) and purged with nitrogen (20 min). The solutions were combined under nitrogen atmosphere and placed in an oil bath at 60 ˚C for 2 hours. The viscous solution was diluted with THF and passed through an aluminum oxide-silica column to remove the copper salts. The polymer solution was concentrated, and the polymer was precipitated twice in hexane from THF. After drying overnight *in vacuo*, 2.98 g of polymer was obtained. The molecular weight of the polymer was determined by size exclusion chromatography (M_n = 9 400 g/mol, PDI = 1.06).

4.4 Loading BNNTs with polymers

The cutting, and loading of BNNTs with PMMA, was conducted as reported previously.[40,41] Cut BNNTs (2.34 mg) were dispersed in a solution of PMMA in THF (200 mg/mL, 2.5 mL) by sonication. The dispersion was cooled in a dry ice/acetone bath for 10 min in a Schlenk flask. The pressure in the flask was then gradually lowered to 1/3 atm using a vacuum pump for two hours. After detaching the flask from the pump, it was left overnight at room temperature to slowly pressurize to atmospheric pressure. The BNNTs were separated by centrifugation, dispersed by a 10 second sonication in a water bath, and washed four times with THF. After drying overnight *in vacuo*, the BNNTs were washed again seven times with THF. After drying *in vacuo*, 2.96 mg of BNNTs loaded with PMMA (BNNT-PMMA) were obtained.

Similarly, BNNTs were loaded with the other polymers: 2.82 mg BNNTs were loaded in 2.7 mL PVP solution (200 mg/mL in methanol), 2.98 mg BNNTs were loaded in 2.7 mL P4VP solution (200 mg/mL in chloroform), and 2.7 mg BNNTs were loaded in 1.0 mL PDR1A solution (200 mg/mL in THF). After loading, all samples were washed at least 10 times with a good solvent for the respective polymer. After drying *in vacuo*, 4.56 mg BNNT-PVP, 5.78 mg BNNT-P4VP, and 5.0 mg BNNT-PDR1A were obtained.

4.5 Instruments and methods

For the IR measurements, the BNNTs were dispersed in 300 μL methanol by sonication. 10 μL of this dispersion was deposited on the ATR crystal and the methanol left to evaporate. Similarly, spectra of pure polymer were measured from a 10 μL drop of the respective polymer solution (200 mg/mL). Spectra were recorded using a Tensor 27 FT-IR spectrometer (Bruker Optics) equipped with a liquid-nitrogen-cooled MCT detector by averaging 100 scans

with a 4 cm^{-1} resolution. Measurements were conducted using a Heated Golden Gate (Specac) diamond ATR accessory. The stage was heated to 160 °C, annealed for 2 minutes, and cooled to 40 °C (2 °C/min) while measuring spectra every 2 °C. Triplicates of most samples were measured. The spectra were collected and analysed with OPUS 6.5 software using 50 % center of gravity in determining the band positions, which is a method providing < 0.01 cm^{-1} uncertainty.[13,21]

Differential scanning calorimetry was performed with a TA Instruments Q2000 DSC, using a 20 °C/min heating rate from 10 to 185 °C (P4VP, PVP) or -90 to 165 °C (PMMA). The samples were equilibrated at the lowest temperature for 10 min before repeating the heating ramp. The thermograms are presented in Supporting Information (Figure S10, S11, and S12). The determination of the T_g of BNNTs loaded with polymers failed, as the signal to noise ratio was too low, due to the small sample sizes available. In this context, using IR to determine a spectroscopic T_g proves advantageous because its chemical selectivity allows probing the polymer band directly.

Transmission electron microscopy (TEM) measurements were conducted on a Tecnai T(12) instrument operating at 80 or 120 kV. The dispersion (2 x 4 µL in methanol) was dropped on carbon Formvar coated 200 mesh copper grids and dried.

For the photoisomerization of PD1RA, a Prizmatix FC5 Multichannel LED (100 mW/cm^2) was used as the light source. The samples were illuminated for 2 min with 450 or 520 nm light before the IR measurements.

The molecular weight of the PMMA was determined using a size exclusion chromatography (SEC) system consisting of an Agilent 1100 isocratic pump, a set of TSK-gel (Tosoh Biosep)

columns, a Dawn EOS multi-angle laser light scattering detector (λ = 690 nm, Wyatt Technology Co.) and an Optilab DSP interferometric refractometer (λ = 690 nm, Wyatt Technology Co.). The eluent was DMF at a flow rate of 0.3 mL/min. The columns temperature was set at 40 °C. For the measurements, we used the reported value of 0.059 mL/g for the dn/dc of PMMA.[87]

Supporting Information

TEM images of boron nitride nanotubes, DSC thermograms, additional IR spectra, and changes in absorbance band position with temperature, are presented as supporting information. Supporting Information is available from the Wiley Online Library or from the author.

Acknowledgements

For financial support, J.N. acknowledges the Department of Chemistry of the University of Montreal (Canada), and J.V. is grateful for funding from Banting Postdoctoral Fellowship (Canada). C.P. acknowledges funding from the Natural Sciences and Engineering Research Council of Canada (NSERC #RGPIN-2015-04014). D.G. is grateful to the Australian Research Council (ARC) for granting a Laureate Fellowship FL160100089.

Dedication

While preparing this paper, Professor Françoise M. Winnik tragically passed away in February, 2021. She will be remembered for her curiosity, excellence, scientific rigor, and her will to take on and tackle new challenges in the fields of amphiphilic materials, polymer chemistry, material science, and the biomedical applications of nanoparticles. She will be greatly missed as a collaborator and mentor, and as a friend.

Received: ((will be filled in by the editorial staff))
Revised: ((will be filled in by the editorial staff))
Published online: ((will be filled in by the editorial staff))

5. References

[1] Z. Usatenko, K. S. Danel, *arXiv:1801.01590 [cond-mat]* **2018**.
[2] P. Romiszowski, A. Sikorski, *J Mol Model* **2005**, *11*, 335.
[3] K. Geng, R. Katsumata, X. Yu, H. Ha, A. R. Dulaney, C. J. Ellison, O. K. C. Tsui, *Macromolecules* **2017**, *50*, 609.
[4] C. J. Ellison, J. M. Torkelson, *Nature Mater* **2003**, *2*, 695.
[5] S. T. Milner, J. E. G. Lipson, *Macromolecules* **2010**, *43*, 9865.
[6] O. K. C. Tsui, T. P. Russell, C. J. Hawker, *Macromolecules* **2001**, *34*, 5535.
[7] J. L. Keddie, R. A. L. Jones, R. A. Cory, *Faraday Discussions* **1994**, *98*, 219.
[8] P. Rittigstein, J. M. Torkelson, *Journal of Polymer Science Part B: Polymer Physics* **2006**, *44*, 2935.
[9] Z. Yang, Y. Fujii, F. K. Lee, C.-H. Lam, O. K. C. Tsui, *Science* **2010**, *328*, 1676.
[10] S. Alexandris, P. Papadopoulos, G. Sakellariou, M. Steinhart, H.-J. Butt, G. Floudas, *Macromolecules* **2016**, *49*, 7400.
[11] B. D. Vogt, *Journal of Polymer Science Part B: Polymer Physics* **2018**, *56*, 9.
[12] R. D. Priestley, C. J. Ellison, L. J. Broadbelt, J. M. Torkelson, *Science* **2005**, *309*, 456.
[13] P. R. Griffiths, J. A. D. Haseth, *Fourier Transform Infrared Spectrometry*, John Wiley & Sons, **2007**.
[14] J. M. Chalmers, P. R. Griffiths, *Handbook of Vibrational Spectroscopy, Volumes 1–5. Edited by J. M. Chalmers and P. R. Griffiths. John Wiley & Sons, Chichester, 2002, p. 3862*, **2001**.
[15] T. Buffeteau, F. Lagugné Labarthet, M. Pézolet, C. Sourisseau, *Macromolecules* **1998**, *31*, 7312.
[16] T. Buffeteau, M. Pézolet, *Appl Spectrosc* **1996**, *50*, 948.
[17] F. L. Labarthet, S. Freiberg, C. Pellerin, M. Pézolet, A. Natansohn, P. Rochon, *Macromolecules* **2000**, *33*, 6815.
[18] W. F. Wolkers, H. Oldenhof, M. Alberda, F. A. Hoekstra, *Biochimica et Biophysica Acta (BBA) - General Subjects* **1998**, *1379*, 83.
[19] K. Tashiro, A. Yoshioka, *Macromolecules* **2002**, *35*, 410.
[20] A. Laventure, G. D. Grandpré, A. Soldera, O. Lebel, C. Pellerin, *Phys. Chem. Chem. Phys.* **2016**, *18*, 1681.
[21] J. Vapaavuori, A. Laventure, C. G. Bazuin, O. Lebel, C. Pellerin, *Journal of the American Chemical Society* **2015**, *137*, 13510.
[22] K. V. Agrawal, S. Shimizu, L. W. Drahushuk, D. Kilcoyne, M. S. Strano, *Nat Nano* **2017**, *12*, 267.
[23] D. Golberg, Y. Bando, Y. Huang, T. Terao, M. Mitome, C. Tang, C. Zhi, *ACS Nano* **2010**, *4*, 2979.
[24] G. Ciofani, S. Del Turco, A. Rocca, G. de Vito, V. Cappello, M. Yamaguchi, X. Li, B. Mazzolai, G. Basta, M. Gemmi, V. Piazza, D. Golberg, V. Mattoli, *Nanomedicine* **2014**, *9*, 773.
[25] L. Horváth, A. Magrez, D. Golberg, C. Zhi, Y. Bando, R. Smajda, E. Horváth, L. Forró, B. Schwaller, *ACS Nano* **2011**, *5*, 3800.
[26] G. Ciofani, S. Danti, G. G. Genchi, B. Mazzolai, V. Mattoli, *Small* **2013**, *9*, 1672.

[27] Z. Li, Z.-A. Li, S. Sun, D. Zheng, H. Wang, H. Tian, H. Yang, X. Bai, J. Li, *Nanomaterials* **2018**, *8*, 86.
[28] J. Chen, M. A. Hamon, H. Hu, Y. Chen, A. M. Rao, P. C. Eklund, R. C. Haddon, *Science* **1998**, *282*, 95.
[29] Y.-T. R. Lau, M. Yamaguchi, X. Li, Y. Bando, D. Golberg, F. M. Winnik, *J. Phys. Chem. C* **2013**, *117*, 19568.
[30] C. Zhi, Y. Bando, C. Tang, D. Golberg, *J. Am. Chem. Soc.* **2005**, *127*, 17144.
[31] S. K. Mudedla, K. Balamurugan, V. Subramanian, *J. Phys. Chem. C* **2016**, *120*, 28246.
[32] G. Ciofani, L. Ricotti, S. Danti, A. A. Menciassi, F. Chiellini, D. D\'Alessandro, S. Moscato, *International Journal of Nanomedicine* **2010**, 285.
[33] X. Chen, P. Wu, M. Rousseas, D. Okawa, Z. Gartner, A. Zettl, C. R. Bertozzi, *J. Am. Chem. Soc.* **2009**, *131*, 890.
[34] X. Wu, W. An, X. C. Zeng, *J. Am. Chem. Soc.* **2006**, *128*, 12001.
[35] A. Rimola, *J. Phys. Chem. C* **2015**, *119*, 17707.
[36] K. Waters, R. Pandey, S. P. Karna, *ACS Omega* **2017**, *2*, 76.
[37] S. Mukhopadhyay, R. H. Scheicher, R. Pandey, S. P. Karna, *J. Phys. Chem. Lett.* **2011**, *2*, 2442.
[38] P. Bilalis, D. Katsigiannopoulos, A. Avgeropoulos, G. Sakellariou, *RSC Advances* **2014**, *4*, 2911.
[39] Y.-T. R. Lau, M. Yamaguchi, X. Li, Y. Bando, D. Golberg, F. M. Winnik, *Langmuir* **2014**, *30*, 1735.
[40] J. Niskanen, I. Zhang, Y. Xue, D. Golberg, D. Maysinger, F. M. Winnik, *Nanomedicine* **2016**, *11*, 447.
[41] J. Niskanen, I. Zhang, Y. Xue, D. Golberg, D. Maysinger, F. M. Winnik, *Materials Today Chemistry* **2020**, *16*, 100270.
[42] D. Abu Saleh, J. Niskanen, Y. Xue, D. Golberg, F. M. Winnik, A. Sosnik, *Materials Today Chemistry* **2017**, *6*, 45.
[43] T. H. Ferreira, A. Marino, A. Rocca, I. Liakos, S. Nitti, A. Athanassiou, V. Mattoli, B. Mazzolai, E. M. B. de Sousa, G. Ciofani, *International Journal of Pharmaceutics* **2015**, *481*, 56.
[44] G. Ciofani, G. G. Genchi, I. Liakos, A. Athanassiou, D. Dinucci, F. Chiellini, V. Mattoli, *Journal of Colloid and Interface Science* **2012**, *374*, 308.
[45] M. Ejaz, S. C. Rai, K. Wang, K. Zhang, W. Zhou, S. M. Grayson, *J. Mater. Chem. C* **2014**, *2*, 4073.
[46] C. Zhi, Y. Bando, C. Tang, H. Kuwahara, D. Golberg, *J. Phys. Chem. C* **2007**, *111*, 1230.
[47] S.-J. Zhou, C.-Y. Ma, Y.-Y. Meng, H.-F. Su, Z. Zhu, S.-L. Deng, S.-Y. Xie, *Nanotechnology* **2012**, *23*, 055708.
[48] A. M. Díez-Pascual, A. L. Díez-Vicente, *RSC Advances* **2016**, *6*, 79507.
[49] S. Kalay, Y. Stetsyshyn, V. Lobaz, K. Harhay, H. Ohar, M. Çulha, *Nanotechnology* **2016**, *27*, 035703.
[50] J. Guan, K. S. Kim, M. B. Jakubinek, B. Simard, *ChemistrySelect* **2018**, *3*, 9308.
[51] M. Emanet, Ö. Şen, Z. Çobandede, M. Çulha, *Colloids and Surfaces B: Biointerfaces* **2015**, *134*, 440.
[52] T. W. Ebbesen, *Journal of Physics and Chemistry of Solids* **1996**, *57*, 951.
[53] V. Chaban, *Chemical Physics Letters* **2010**, *500*, 35.
[54] E. Abdullayev, R. Price, D. Shchukin, Y. Lvov, *ACS Appl. Mater. Interfaces* **2009**, *1*, 1437.
[55] D. G. Shchukin, S. V. Lamaka, K. A. Yasakau, M. L. Zheludkevich, M. G. S. Ferreira, H. Mohwald, *J. Phys. Chem. C* **2008**, *112*, 958.
[56] D. Fix, D. V. Andreeva, Y. M. Lvov, D. G. Shchukin, H. Möhwald, *Adv. Funct. Mater.* **2009**, *19*, 1720.

[57] J. Vapaavuori, I. T. S. Heikkinen, V. Dichiarante, G. Resnati, P. Metrangolo, R. G. Sabat, C. G. Bazuin, A. Priimagi, C. Pellerin, *Macromolecules* **2015**, *48*, 7535.
[58] E. Groppo, M. J. Uddin, O. Zavorotynska, A. Damin, J. G. Vitillo, G. Spoto, A. Zecchina, *J. Phys. Chem. C* **2008**, *112*, 19493.
[59] X. Wang, C. G. Bazuin, C. Pellerin, *Polymer* **2015**, *57*, 62.
[60] C. Zhi, Y. Bando, C. Tang, D. Golberg, R. Xie, T. Sekigushi, *Appl. Phys. Lett.* **2005**, *86*, 213110.
[61] T. Ikuno, T. Sainsbury, D. Okawa, J. M. J. Fréchet, A. Zettl, *Solid State Communications* **2007**, *142*, 643.
[62] L. Gilburd, X. G. Xu, Y. Bando, D. Golberg, G. C. Walker, *J. Phys. Chem. Lett.* **2016**, *7*, 289.
[63] L.-T. Lee, E. M. Woo, S. S. Hou, S. Förster, *Polymer* **2006**, *47*, 8350.
[64] Ye. D. Vorontsov, V. P. Panov, *Polymer Science U.S.S.R.* **1976**, *18*, 2752.
[65] C. Zhi, Y. Bando, C. Tang, R. Xie, T. Sekiguchi, D. Golberg, *J. Am. Chem. Soc.* **2005**, *127*, 15996.
[66] C. Y. Zhi, Y. Bando, C. C. Tang, Q. Huang, D. Golberg, *Journal of Materials Chemistry* **2008**, *18*, 3900.
[67] S. A. Curran, P. M. Ajayan, W. J. Blau, D. L. Carroll, J. N. Coleman, A. B. Dalton, A. P. Davey, A. Drury, B. McCarthy, S. Maier, A. Strevens, *Advanced Materials* **1998**, *10*, 1091.
[68] J. N. Coleman, A. B. Dalton, S. Curran, A. Rubio, A. P. Davey, A. Drury, B. McCarthy, B. Lahr, P. M. Ajayan, S. Roth, R. C. Barklie, W. J. Blau, *Advanced Materials* **2000**, *12*, 213.
[69] E. J. Mele, P. Král, *Phys. Rev. Lett.* **2002**, *88*, 056803.
[70] N. Jiang, M. Sen, M. K. Endoh, T. Koga, E. Langhammer, P. Bjöörn, M. Tsige, *Langmuir* **2018**, *34*, 4199.
[71] N. Jiang, J. Cheung, Y. Guo, M. K. Endoh, T. Koga, G. Yuan, S. K. Satija, *Macromolecular Chemistry and Physics* **2018**, *219*, 1700326.
[72] S. Napolitano, M. Wübbenhorst, *Nat Commun* **2011**, *2*, 260.
[73] O. K. C. Tsui, H. F. Zhang, *Macromolecules* **2001**, *34*, 9139.

[74] P. D. Topham, A. Glidle, D. T. W. Toolan, M. P. Weir, M. W. A. Skoda, R. Barker, J. R. Howse, *Langmuir* **2013**, *29*, 6068.
[75] H. Li, C. P. Tripp, *Langmuir* **2004**, *20*, 10526.
[76] D. Li, J. Brisson, *Polymer* **1998**, *39*, 793–800.

[77] M. D. P. Buera, G. Levi, M. Karel, *Biotechnology Progress* **1992**, *8*, 144.
[78] S. M. Taghizadeh, H. Mirzadeh, M. Barikani, M. Yousefi, *International Journal of Adhesion and Adhesives* **2009**, *29*, 302.
[79] J. Wachtveitl, T. N ägele, B. Puell, W. Zinth, M. Krüger, S. Rudolph-Böhner, D. Oesterhelt, L. Moroder, *Journal of Photochemistry and Photobiology A: Chemistry* **1997**, *105*, 283.
[80] J. Zhang, J. Zhao, H. L. Zhang, H. L. Li, Z. F. Liu, *Chemical Physics Letters* **1997**, *271*, 90.
[81] Z. Gao, C. Zhi, Y. Bando, D. Golberg, T. Serizawa, *J. Am. Chem. Soc.* **2010**, *132*, 4976.
[82] J. Chen, L. Li, D. Zhou, X. Wang, G. Xue, *Phys. Rev. E* **2015**, *92*, 032306.
[83] J. Niskanen, A. J. Peltekoff, J.-R. Bullet, B. H. Lessard, F. M. Winnik, *Macromolecules* **2021**, *54*, 6678.

[84] K. Matyjaszewski, *Macromolecules* **2012**, *45*, 4015.

[85] O. N. Tretinnikov, K. Ohta, *Macromolecules* **2002**, *35*, 7343.
[86] X. Wang, C. G. Bazuin, C. Pellerin, *Vibrational Spectroscopy* **2014**, *71*, 18.
[87] Y. Shimura, *BCSJ* **1967**, *40*, 273.

Probing interfacial interactions and dynamics of polymers enclosed in boron nitride nanotubes

ToC figure:

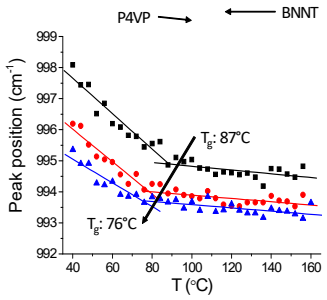

Supporting Information

Probing interfacial interactions and dynamics of polymers enclosed in boron nitride nanotubes

*Jukka Niskanen, Yanming Xue, Dmitri Golberg, Françoise M. Winnik, Christian Pellerin, and Jaana Vapaavuori**

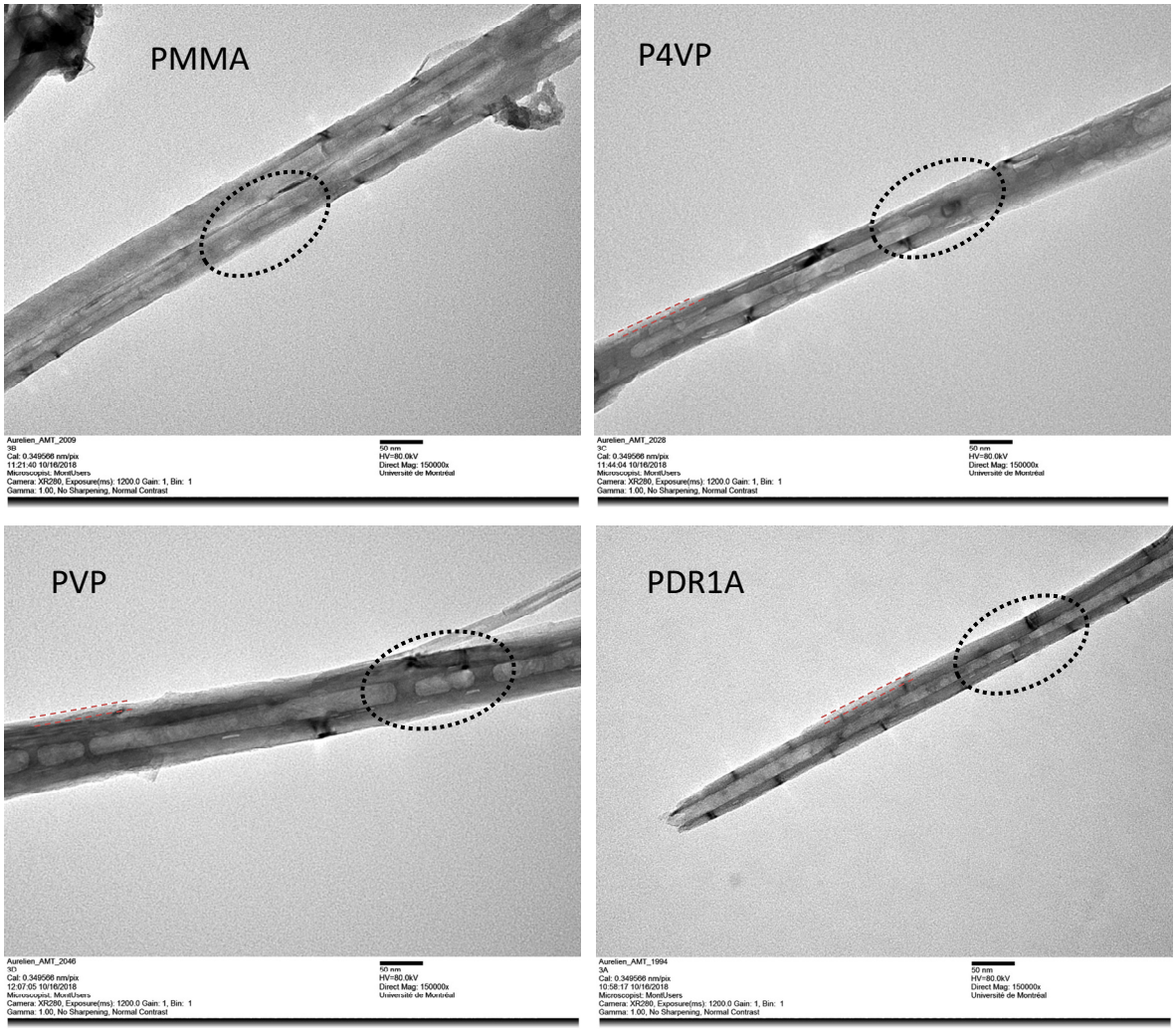

Figure S1. TEM micrograph of BNNTs loaded with PMMA, P4VP, PVP, and PDR1A. Polymer inside the BNNTs is indicated by the black ovals and a thin polymer layer outside the BNNTs by dashed red lines (P4VP, PVP, and PDR1A).

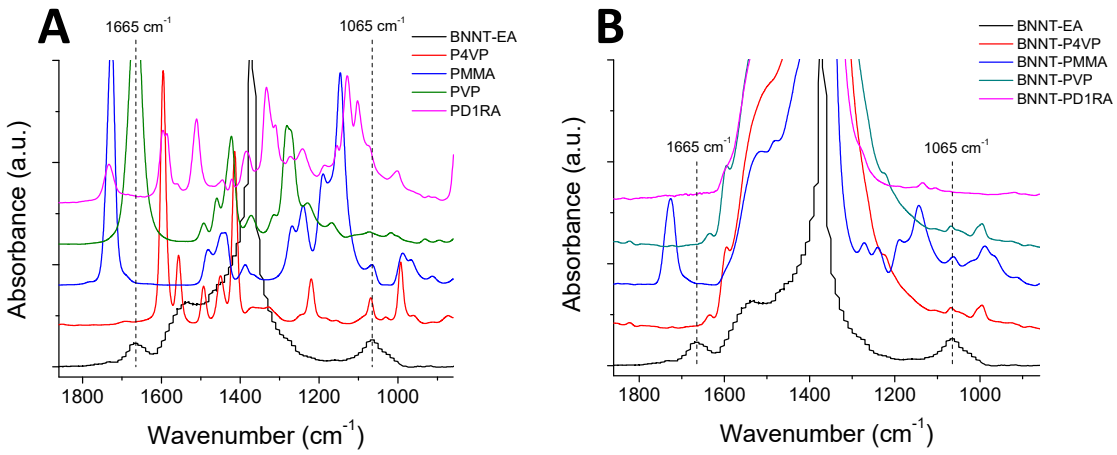

Figure S2. IR spectra of (A) ethanol amine-BNNTs compared with the polymers and (B) ethanol amine-BNNTs compared with BNNTs loaded with the polymers. The absorbance bands for N-H at 1665 cm^{-1} and C-N at 1065 $cm^{-1}$from the ethanolamine are indicated by dashed lines.

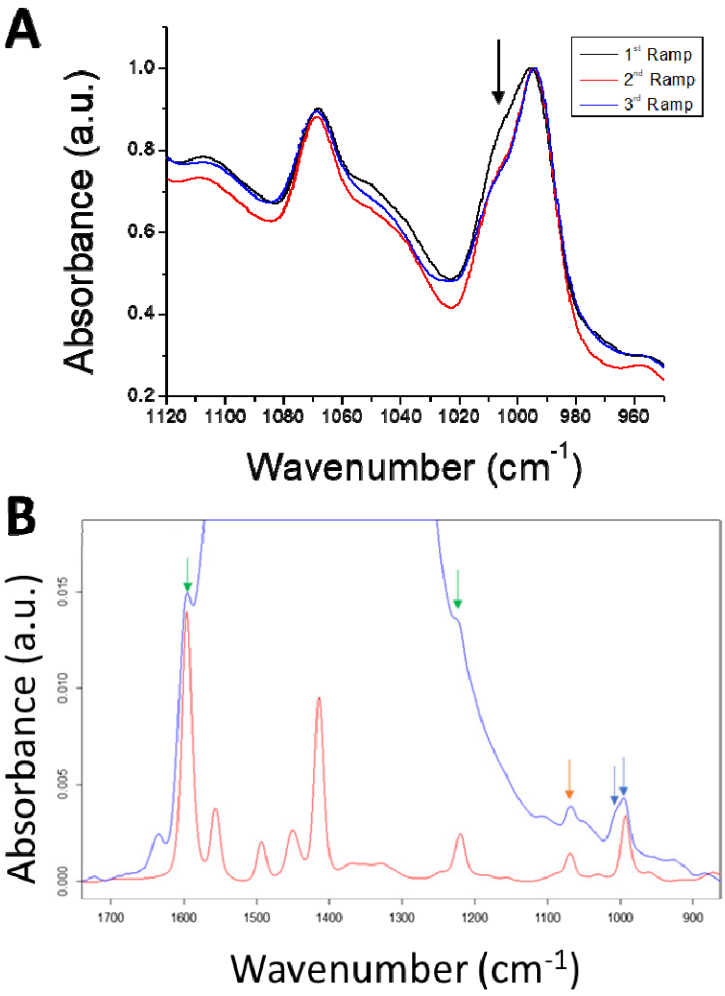

Figure S3. (A) IR spectra of BNNT-P4VP showing the decrease of the 1008 cm^{-1} shoulder, marked by an arrow, of the 993 cm^{-1} band with increasing number of heating cycles. **(B)** Close-up view comparing the spectra of pure P4VP and BNNT-P4VP. The 993 cm^{-1} band and the 1008 cm^{-1} shoulder can be easily distinguished (blue arrows) and several other P4VP bands can be noted, such as the weaker band at 1069 cm^{-1} (red arrow). The 1220 and 1593 cm^{-1} bands are also clearly present (green arrows) even though they are overlapped with the strong BNNT absorption.

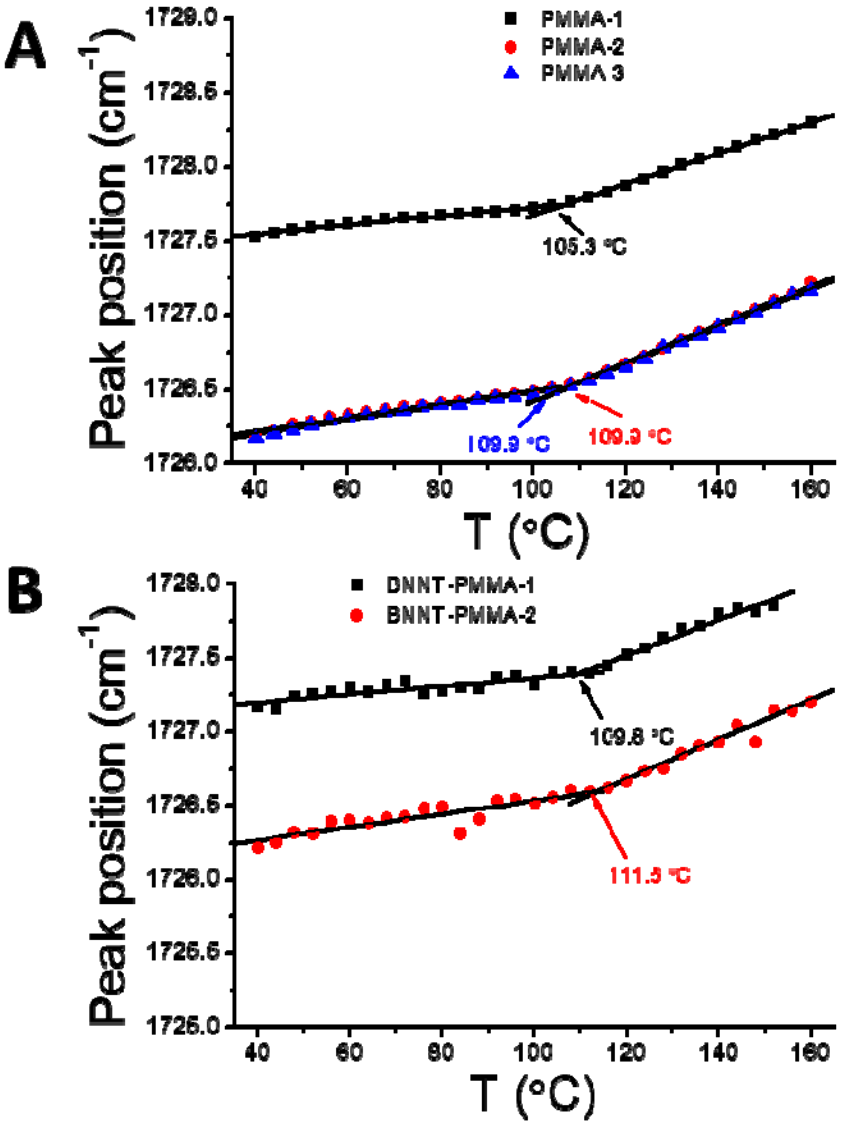
A
PMMA-1
PMMA-2
PMMA 3
Peak position (cm-1)
1729.0
1728.5
1728.0
1727.5
1727.0
1726.5
1726.0
105.3 °C
109.9 °C
109.9 °C
40
60
80
100
120
140
160
T (°C)
B
DNNT-PMMA-1
BNNT-PMMA-2
Peak position (cm-1)
1728.0
1727.5
1727.0
1726.5
1726.0
1725.5
1725.0
109.8 °C
111.9 °C
40
60
80
100
120
140
160
T (°C)
C
BNNT-PMMA
PMMA
Intensity (a.u.)
0.55
0.54
0.53
0.52
0.51
0.5
0.49
0.48
0.47
0.46
0.0235
0.0230
0.0225
0.0220
0.0215
0.0210
0.0205
40
60
80
100
120
140
160
T (°C)

Figure S4. Position of the carbonyl band for PMMA (A) and BNNT-PMMA (B) as a function of temperature for three samples, determined using the center of gravity of the band. For comparison, the intensity of the carbonyl stretching band for PMMA (orange and black) and BNNT-PMMA (red) is shown as a function of temperature for three samples determined (C): The band intensity and band position approaches provide consistent results, as the spectroscopic T_g obtained from the band intensities for PMMA is 104 °C compared to 108 ± 3 °C for the band positions. The result for the BNNT-PMMA also shows a change of slope but the intensity data is much noisier and does not form a straight line at high temperatures, making an estimation of T_g difficult. In fact, the changes in intensity are less than 0.002 absorbance units, which highlights the challenge of using band intensities and justifies our choice of analyzing peak positions for very weak spectra. [1,2,3]

Thanks to the use of a reference laser, the high precision in the determination of the optical retardation in the interferometer converts, after Fourier transformation, into a very high frequency precision in the spectrum. Hence, even at a moderate 4 cm^{-1} resolution, the precision and accuracy of each point in the spectrum is much higher than their separation. The wavenumber accuracy test of our spectrometer, which uses the absorption of a rovibrational water vapor band, indicated deviations of ±0.001 cm^{-1} from the reference value. When the position of a reasonably isolated band is determined using the center of gravity method, which employs the intensity of several points as opposed to a single maximum point,[13,21] the advantage of the frequency precision and accuracy is fully expressed and allows following small band shifts that are well below the spectral resolution of the instrument (Supporting Information, Figure S4C).

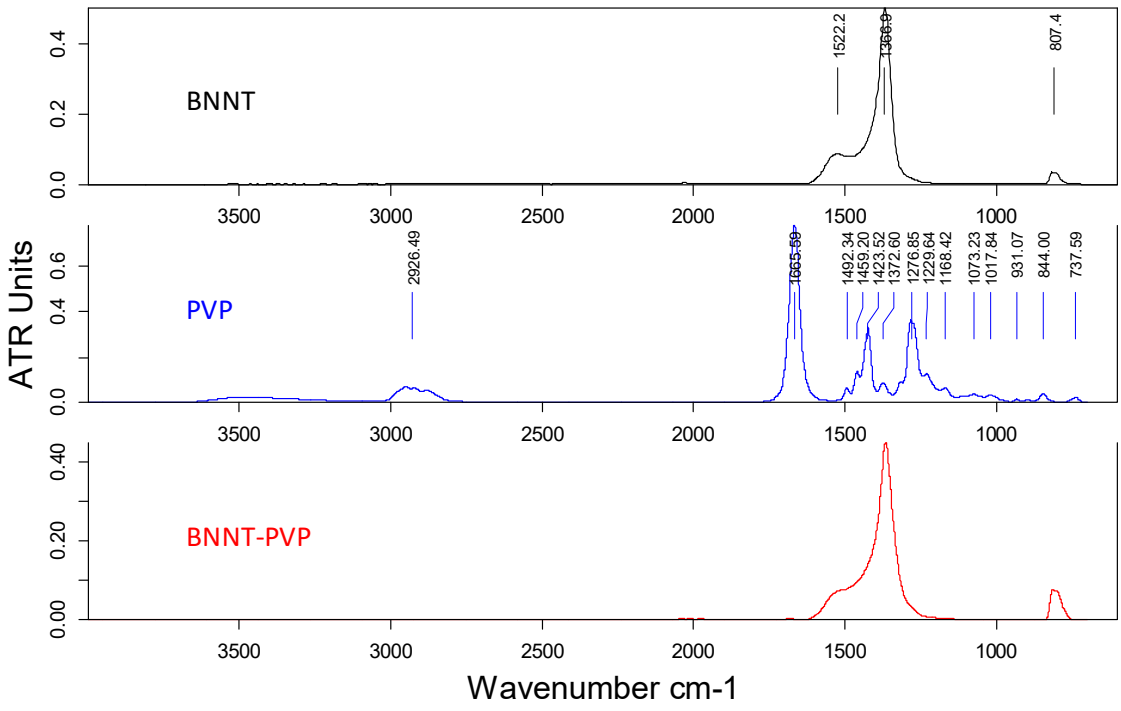

Figure S5. IR spectra of BNNTS, PVP, and BNNT-PVP.

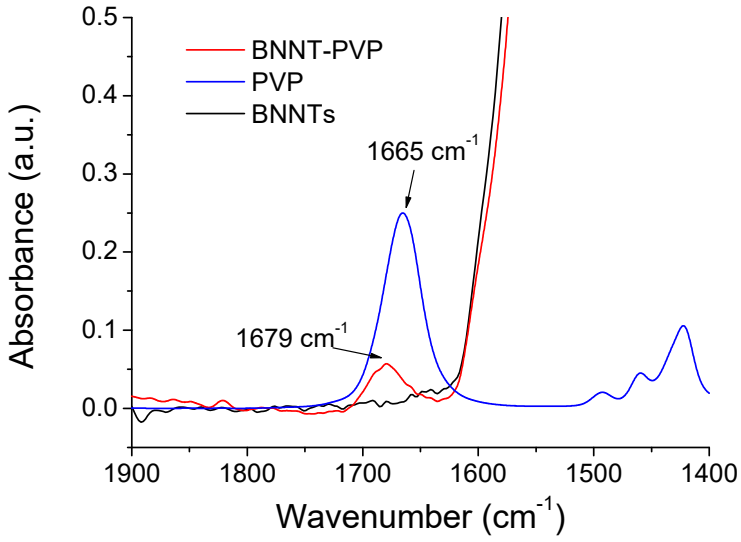

Figure S6. The Amide I band in PVP significantly shifts when the polymer is in BNNTs, indicating hydrogen bonding the polymer with residual water.

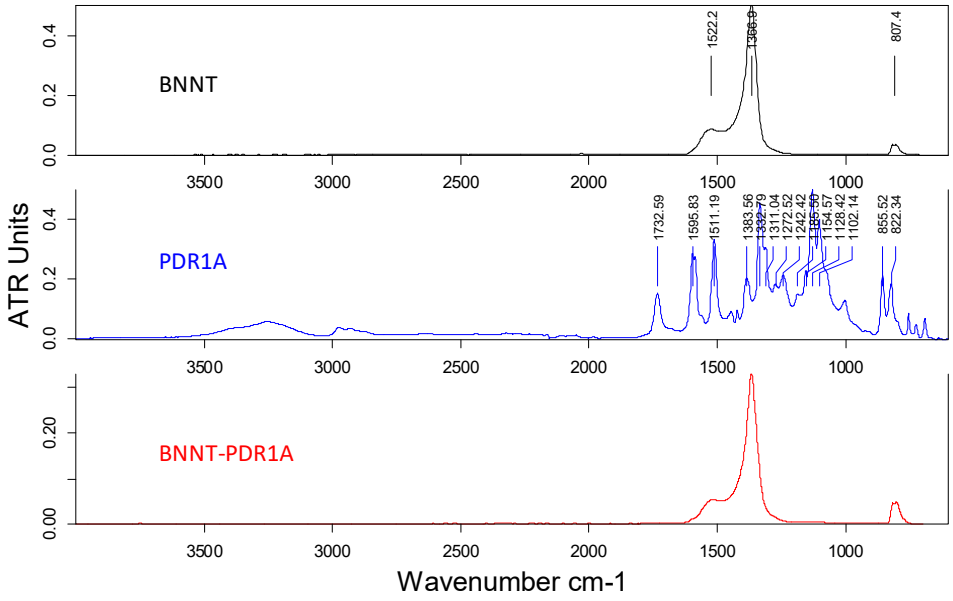

Figure S7. IR spectra of BNNTs, PDR1A, and BNNT-PDR1A.

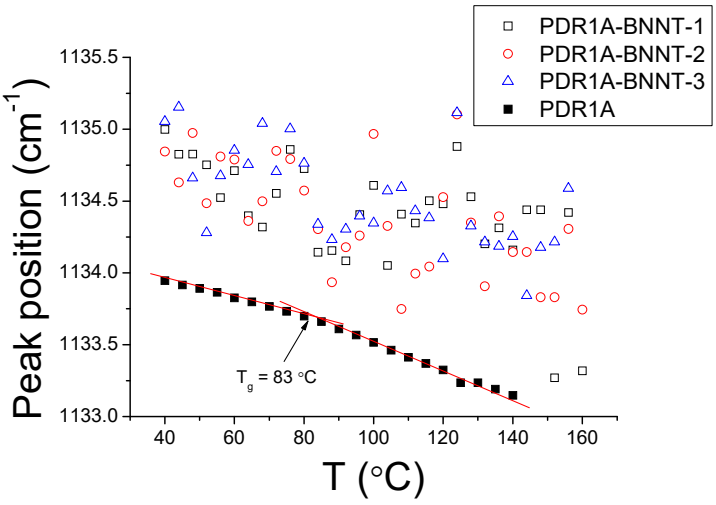

Figure S8. The C-H in-plane bending and ring deformation absorbance band position of PDR1A. The T_g for PDR1A-BNNTs can not be observed from the measurements.

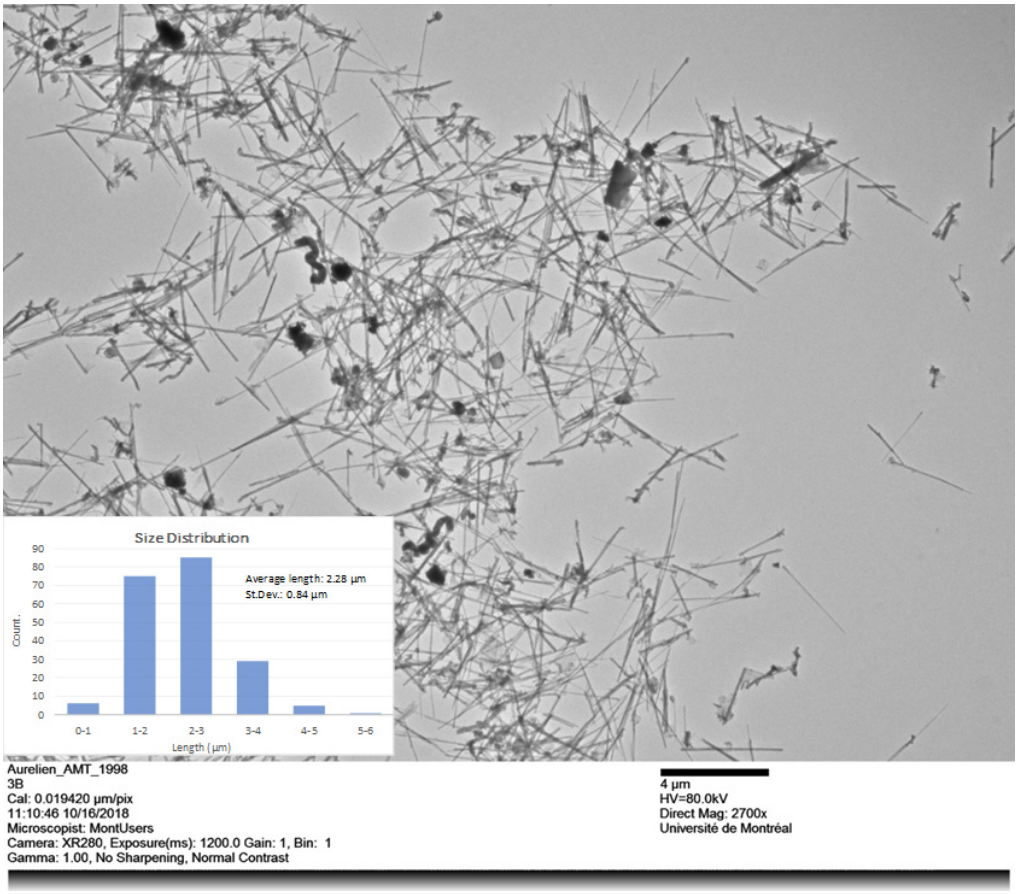

Figure S9. TEM micrograph of BNNTs loaded with PMMA with size distribution.

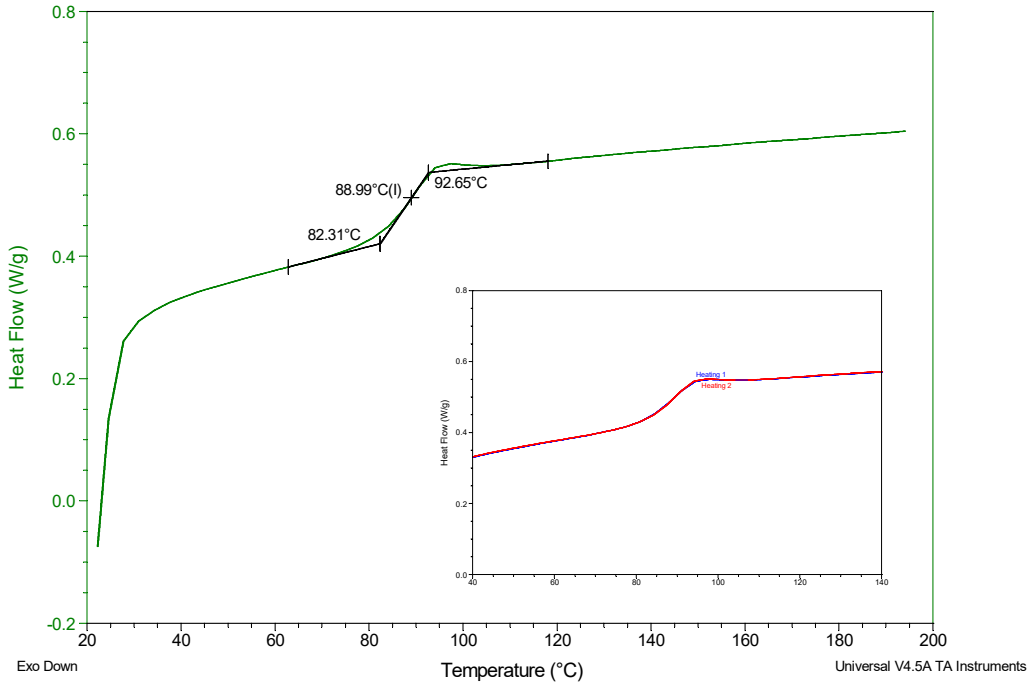

Figure S10. DSC thermogram of P4VP. Two consequent runs are shown in the insert.

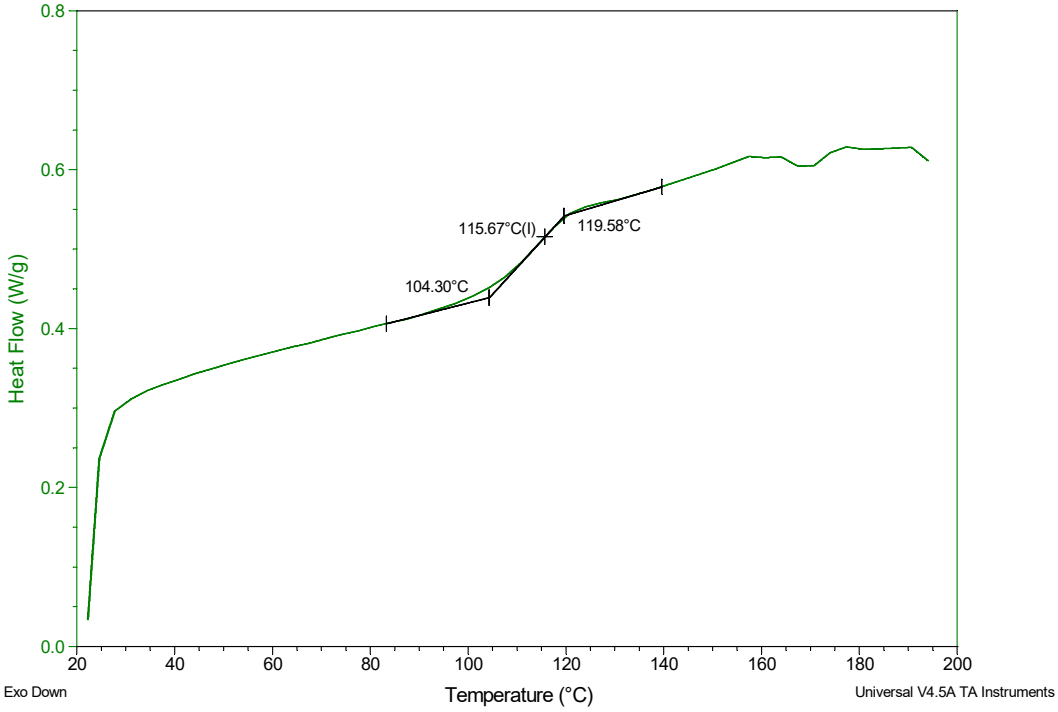

Figure S11. DSC thermogram of PVP.

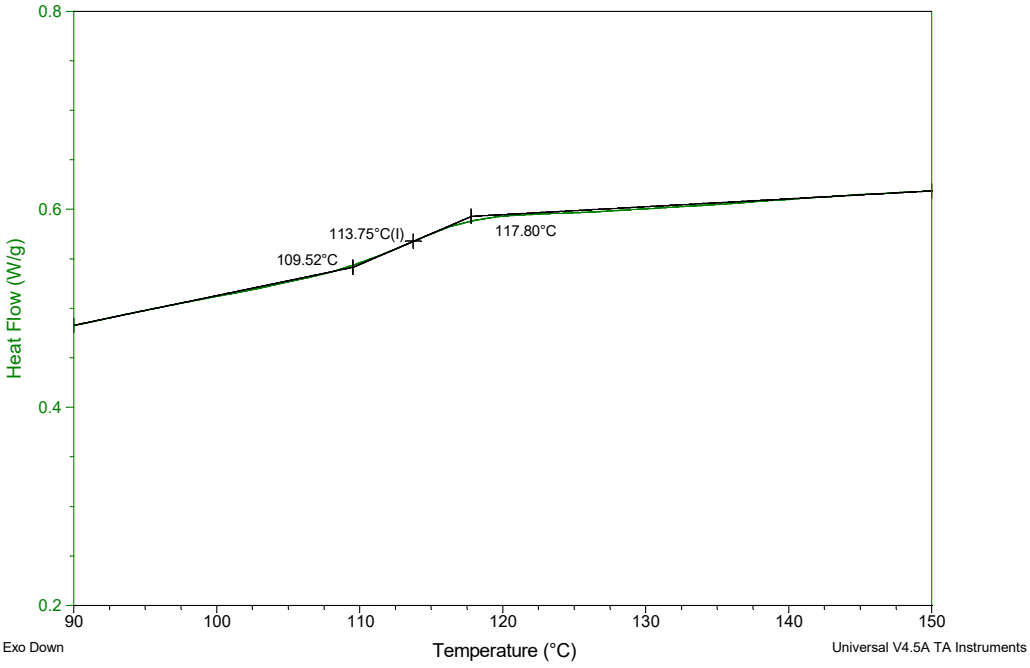

Figure S12. DSC thermogram of PMMA.

References

[1] J. Vapaavuori, A. Laventure, C. G. Bazuin, O. Lebel, C. Pellerin, *Journal of the American Chemical Society* **2015**, *137*, 13510.
[2] O. N. Tretinnikov, K. Ohta, *Macromolecules* **2002**, *35*, 7343.
[3] X. Wang, C. G. Bazuin, C. Pellerin, *Vibrational Spectroscopy* **2014**, *71*, 18.